Assessment of AHI Level-1 Data for HWRF Assimilation

Xiaolei Zou[1] and Fuzhong Weng[2]

[1]Earth System Science Interdisciplinary Center,
University of Maryland, College Park, Maryland

[2]Satellite Meteorology and Climatology Division, NOAA
NESDIS Center for Satellite Applications and Research,

The Sixth Asia/Oceania Meteorological Satellite Users' Conference,
Tokyo, Japan, November 9-13, 2015

Outline

- Concept on Satellite Data Assimilation (DA)
- A Baseline HWRF System for Satellite DA
- Impacts of GOES Imager Radiance Assimilation on Hurricane Track and Intensity Forecasts
- Assessment of AHI Data Applications to HWRF DA
- Summary and Conclusions

Concept of Satellite Data Assimilation

A process of incorporating all observations into weather forecast models to produce the "*best*" description of the atmospheric state at a desired resolution. Physical understanding of observations and weather structures and applicable mathematical optimal control and statistical estimate theories that match computer capabilities and are important for any success of satellite data assimilation.

$$J(\mathbf{x}) = \frac{1}{2}(\mathbf{x}-\mathbf{x}_b)^T \mathbf{B}^{-1}(\mathbf{x}-\mathbf{x}_b) + \frac{1}{2}(H(\mathbf{x})-\mathbf{y}^{obs}-\mu)^T(\mathbf{O}+\mathbf{F})^{-1}(H(\mathbf{x})-\mathbf{y}^{obs}-\mu)$$

$$J(\mathbf{x}_a) = \min_{\mathbf{x}} J(\mathbf{x}) \quad \forall \mathbf{x} \text{ near } \mathbf{x}_b$$

<— Maximum likelihood Estimate

- $\mathbf{x}$ – analysis variable
- $\mathbf{x}_a$ – final analysis
- $\mathbf{x}_b$ – background
- $\mathbf{B}$ – background error covariance

- μ — bias
- $\mathbf{y}^{obs}$ – observations
- $\mathbf{O}$ – observation error covariance
- H – observation operator
- $\mathbf{F}$ – forward model error covariance

The success of satellite DA of any instruments requires the science of satellite data and NWP be effectively integrated together into a DA system and the results from the DA system be carefully analyzed and interpreted.

A Baseline HWRF System for Satellite Data Assimilation

- 2012 NCEP-trunk version 934 HWRF (three nested domains)
- System Modifications
  - Higher model top (0.5 hPa, 61 levels)
  - Warm start
  - Asymmetric vortex initialization
- Advanced POES and GOES DA
  - POES sounding instruments: AMSU, ATMS, CrIS, IASI, AIRS
  - New quality control (QC) for MHS
  - GOES-13/15 imager radiance
  - POES microwave imager radiance (AMSR2, GMI)
  - Surface sensitive channels through Community Surface Emissivity Model (CSEM)

Model Domains

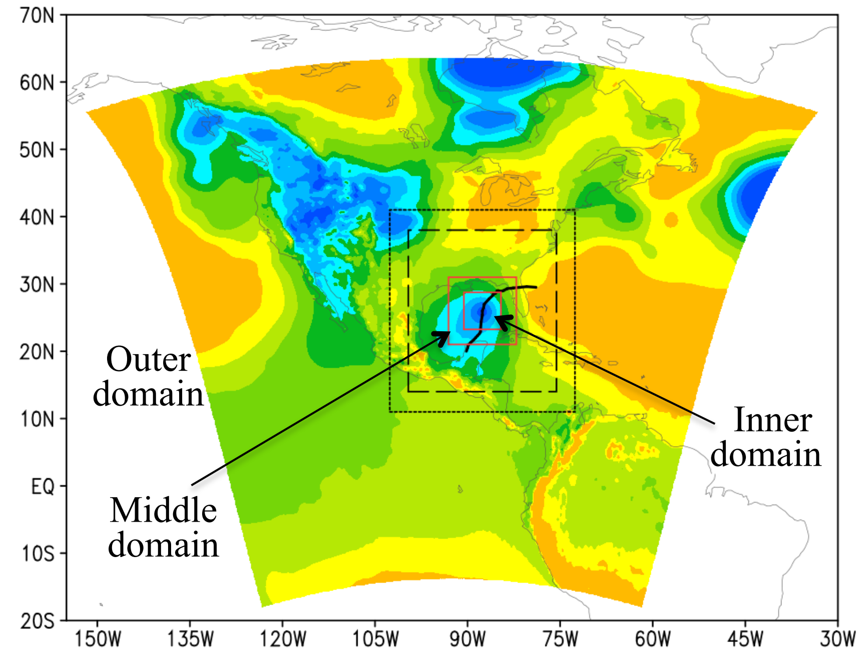

Three telescoping model domains:

Outer domain: 27 km (fixed)

Middle domain: 9 km (moving)

Inner domain: 3 km (moving)

A Newly Added Asymmetric Bogus Vortex to HWRF

Symmetric Vortex

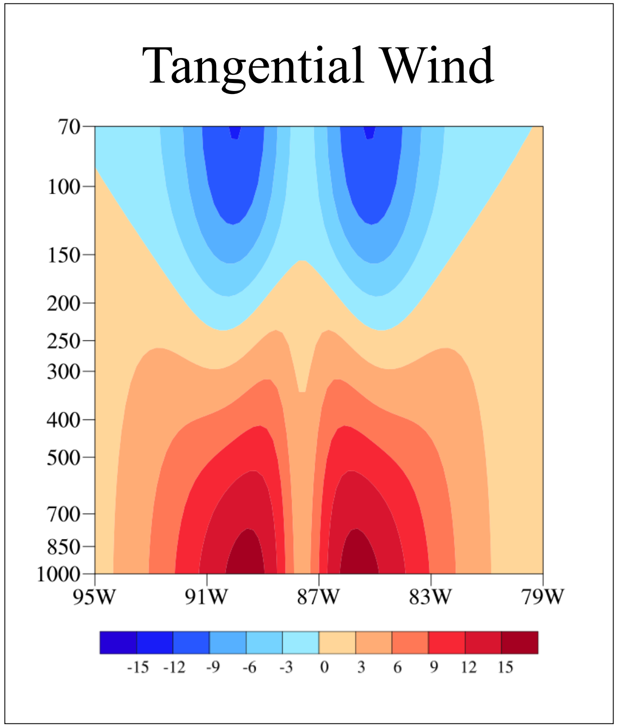

Operational HWRF

Asymmetric Vortex

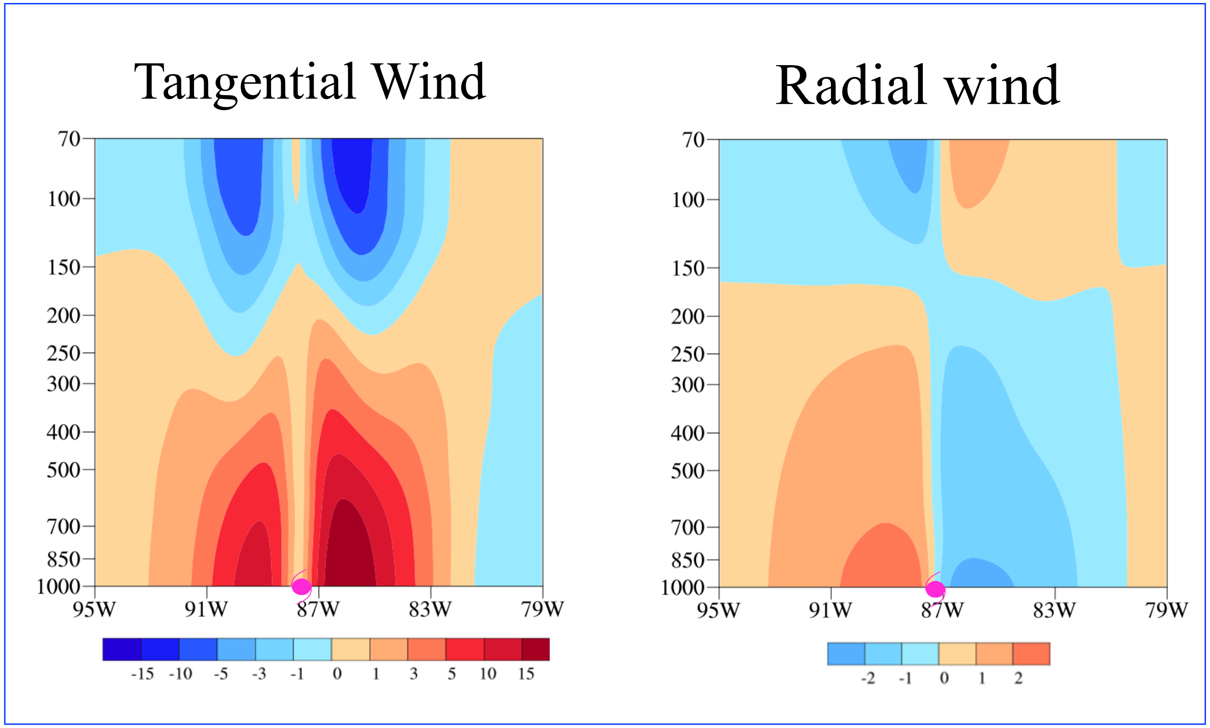

Baseline HWRF/DA System

Tropical storm Debby at 1800 UTC June 23, 2012

GOES-13/15 Imager Channel Characteristics

Channel	Central Frequency (μm)	Band Width (μm)	Spatial Resolution (km)		Observation Error (K)	
			GOES-13	GOES-15	GOES-13	GOES-15
1	0.65	0.19	1.0	1.0	±5%	±5%
2	3.90	0.34	4.0	4.0	0.051	0.063
3	6.55	1.50	4.0	4.0	0.140	0.170
4	10.7	1.00	4.0	4.0	0.053	0.059
6	13.35	0.70	8.0	4.0	0.061	0.130

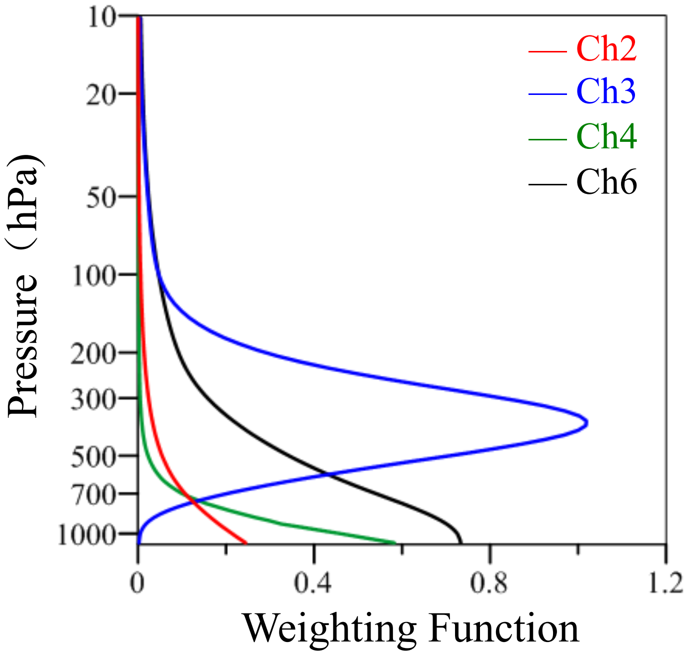

- Imager channels 2-4 are to assimilated in NCEP GSI system
- GOES channel 5 (12.0 μm) had been changed to channel 6 (13.35 μm) since the launch of GOES-12

GOES-13/15 DA with an Asymmetric Vortex Initialization

Channel 3 Data Assimilated after QC

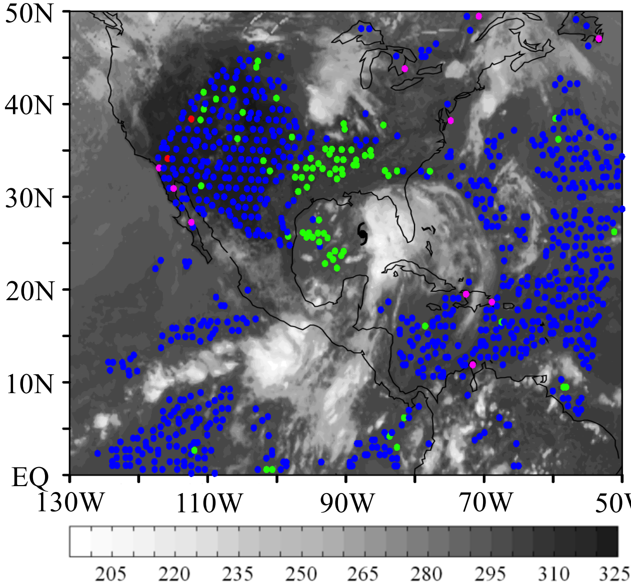

• GOES-13 data assimilated

• • • GOES-13 data eliminated by QC

Asymmetric Relative Vorticity

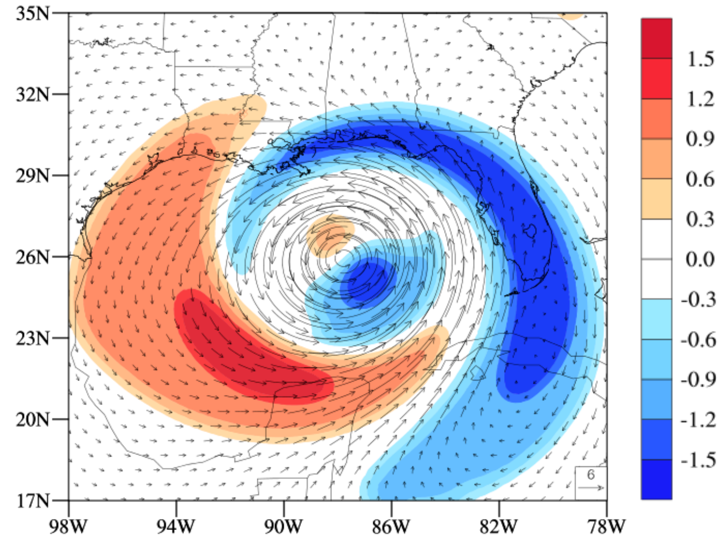

Analysis Difference

$$\Phi^{GOES\ DA}_{ana,300\,hPa} - \Phi^{without\ GOES}_{300\,hPa}$$

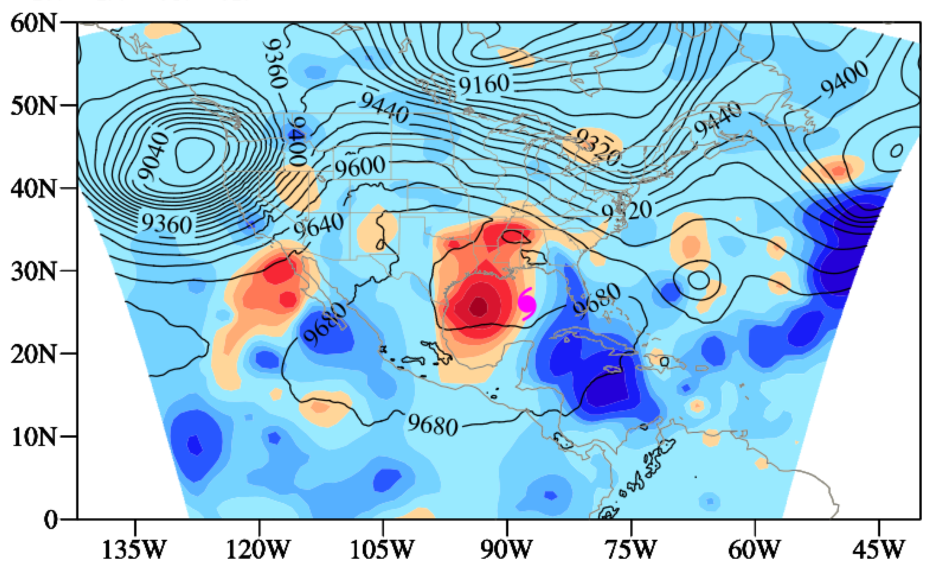

Tropical Storm Debby at 1800 UTC June 23, 2012

Impacts of GOES-13/15 Imager Radiance DA on Track Prediction

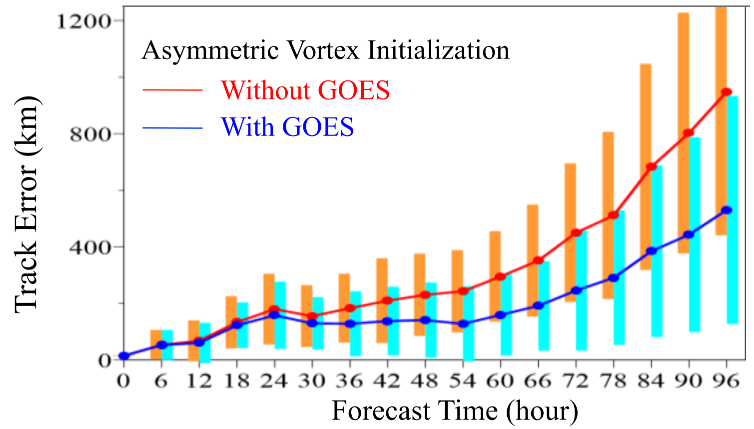

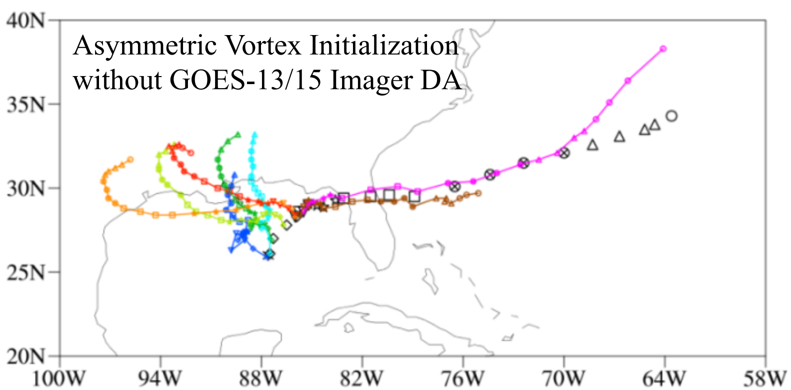

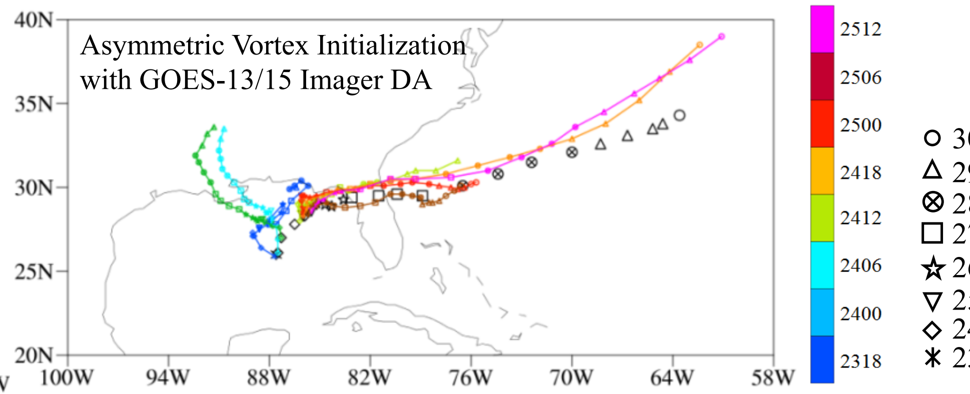

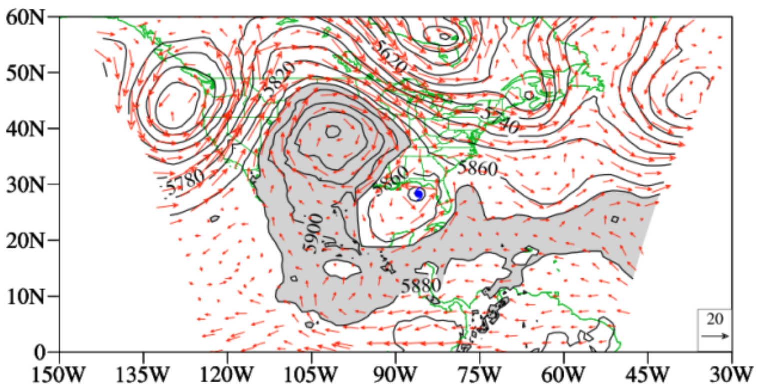

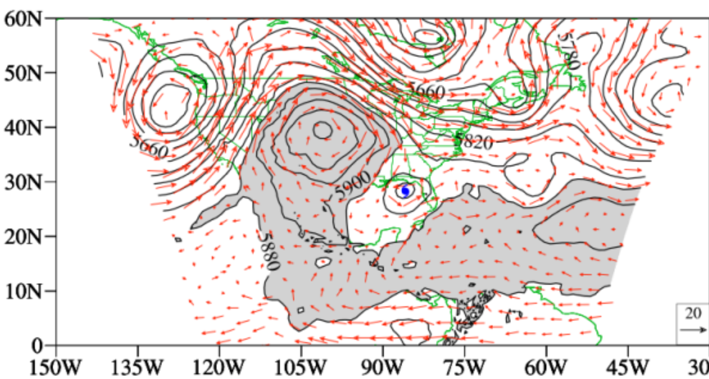

$\Phi^{24\text{-h fcst}}_{500\,hPa}$

valid at 1800 UTC
June 24, 2012

Zou, X., Z. Qin and Y. Zheng, 2015: Improved tropical storm forecasts with GOES-13/15 imager radiance assimilation and asymmetric vortex initialization in HWRF. *Mon. Wea. Rev.*, **143**(7), 2485-2505.

Impacts of GOES-13/15 Imager Radiance DA on Intensity Forecasts

Central Sea-Level Pressure (SLP)

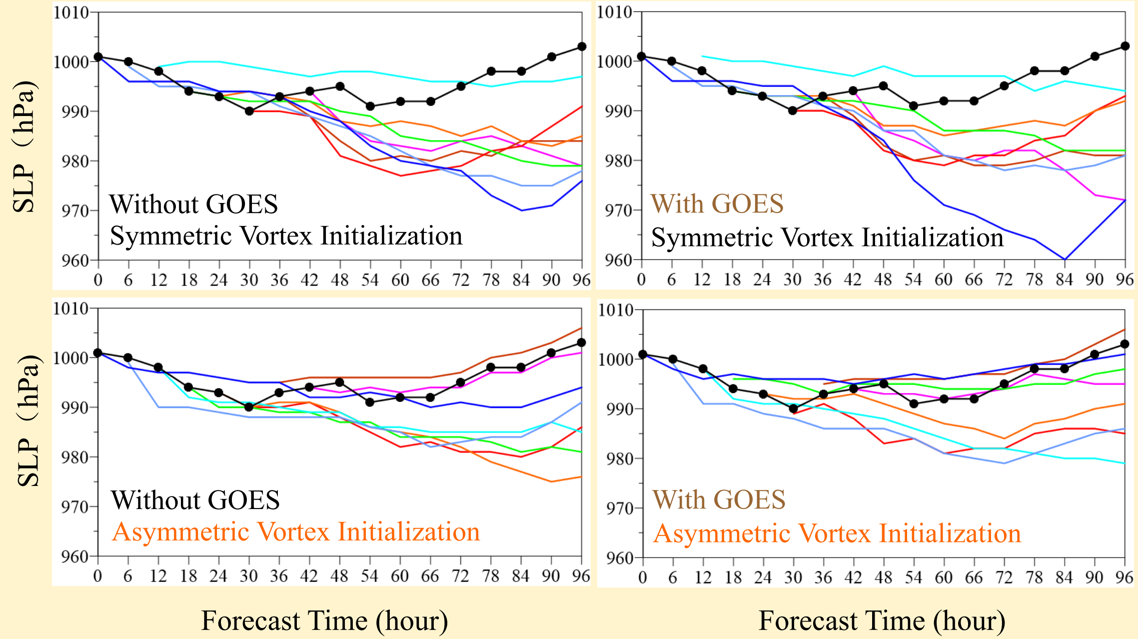

Maximum Surface Wind Speed (V_{max})

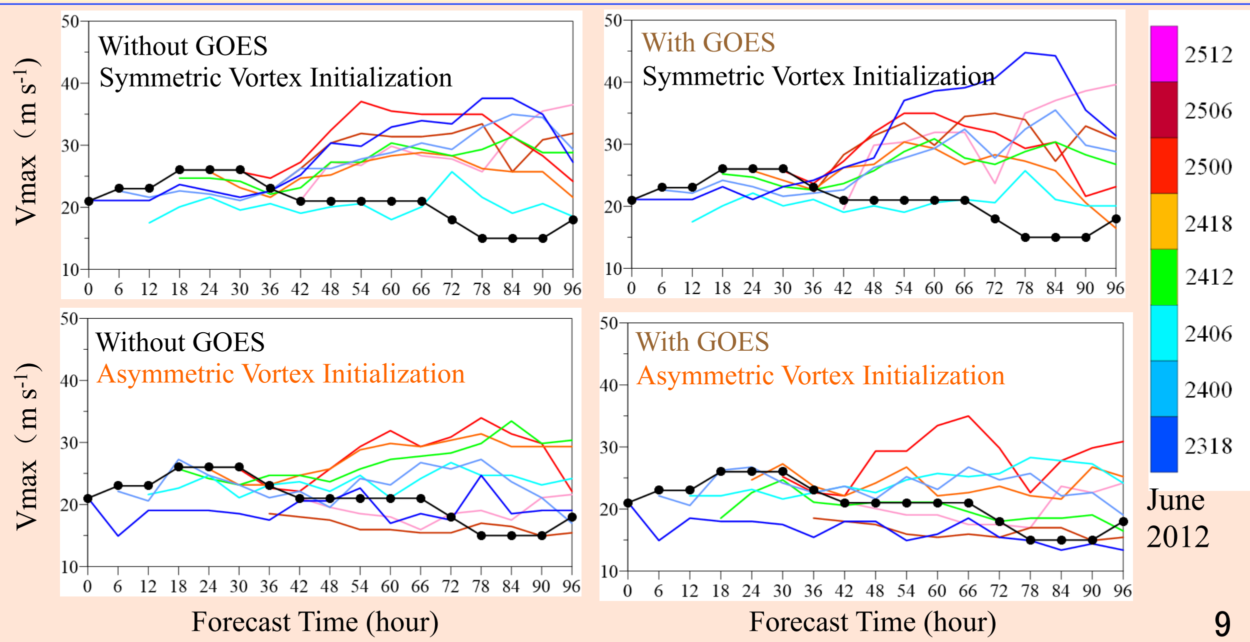

Impacts of GOES-11/-12 Imager Radiance DA on QPFs

- The added impacts of GOES imager radiance DA to different types of satellite data (AMSU-A, HIRS/4, HIRS/3, GSN, AIRS, MHS) was consistently positive on QPFs
- The analysis and forecast errors are significantly reduced by GOES imager radiance DA when verified with independent observations from GOES sounders and AIRS

Threat Scores of 3-h Accumulative Rainfall Averaged over 24 Hours

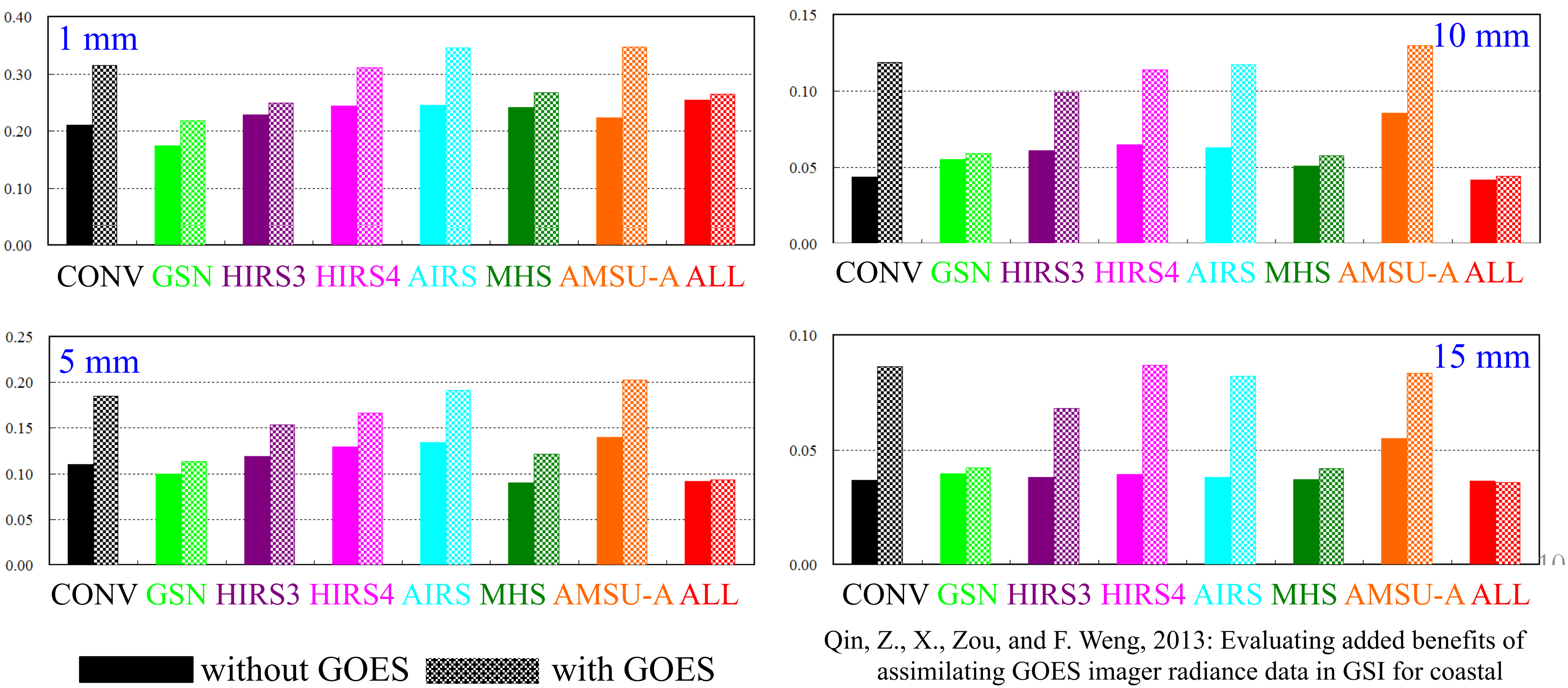

Qin, Z., X., Zou, and F. Weng, 2013: Evaluating added benefits of assimilating GOES imager radiance data in GSI for coastal QPFs. *Mon. Wea. Rev.*, **141**(1), 75-92.

Himawari-8 AHI Channels 7-16

Channel Number	Central Wavelength
7	3.9 mm
8	6.2 mm
9	6.9 mm
10	7.3 mm
11	8.6 mm
12	9.6 mm
13	10.4 mm
14	11.2 mm
15	12.4 mm
16	13.3 mm

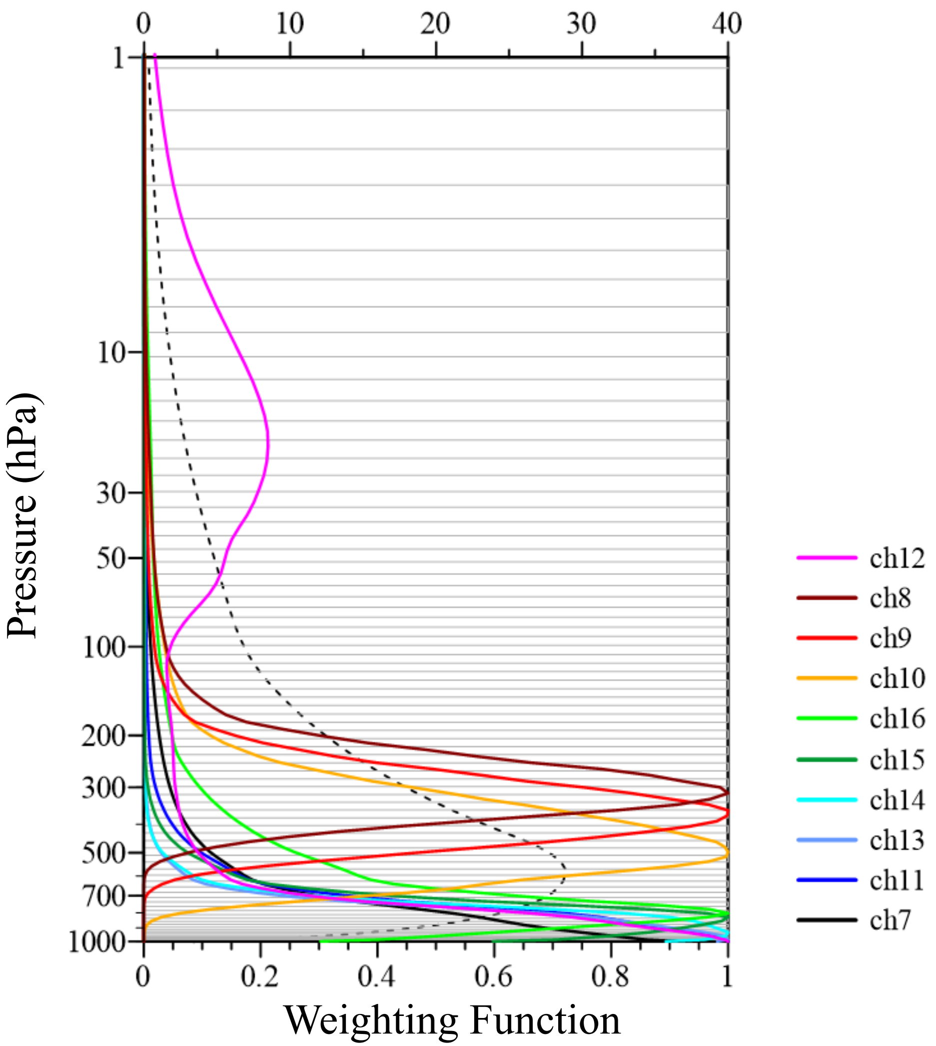

AHI Data

0130 UTC
August 4, 2015

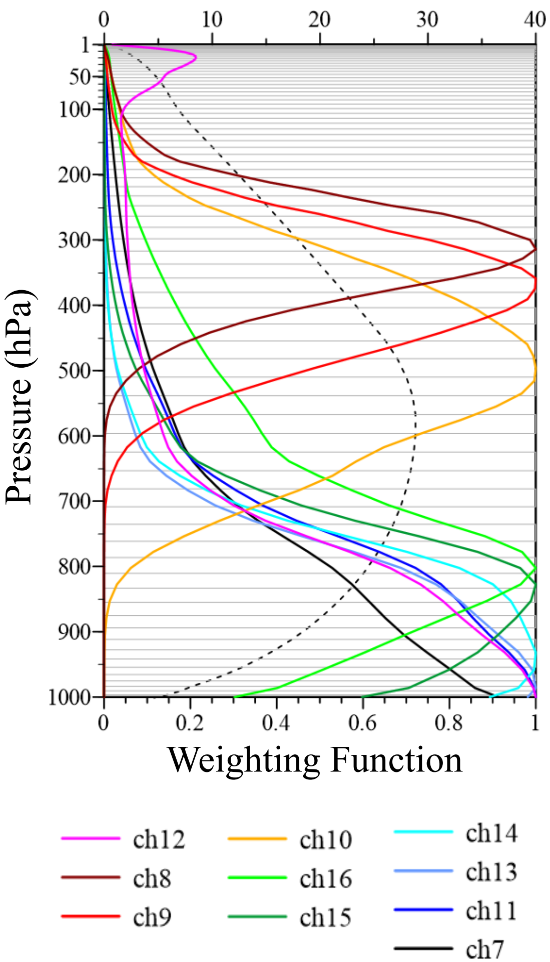

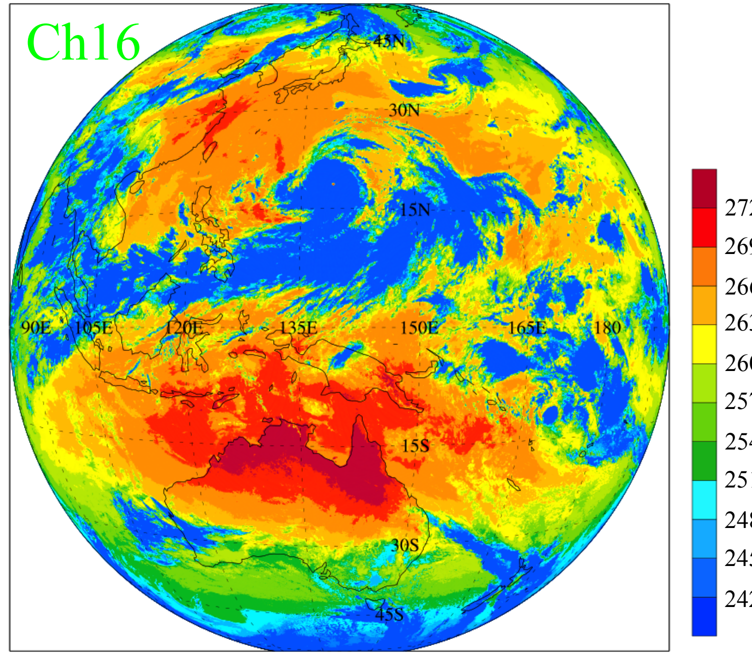

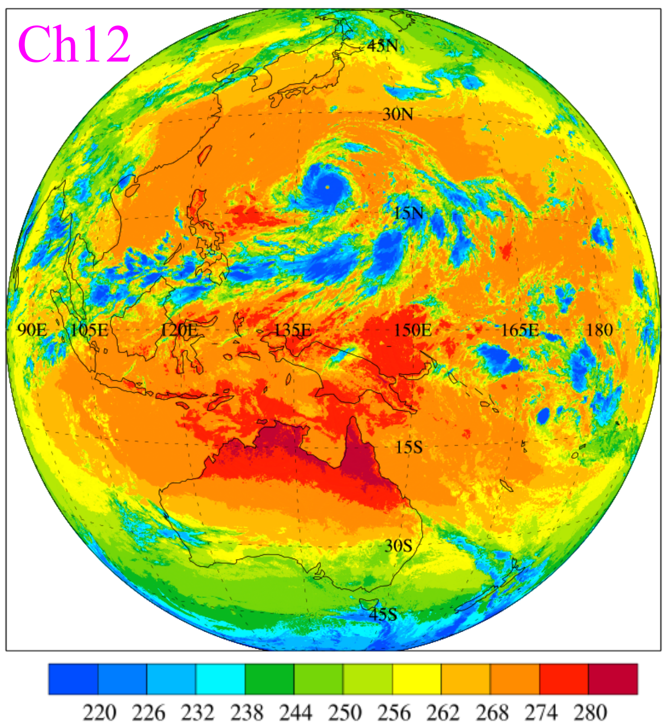

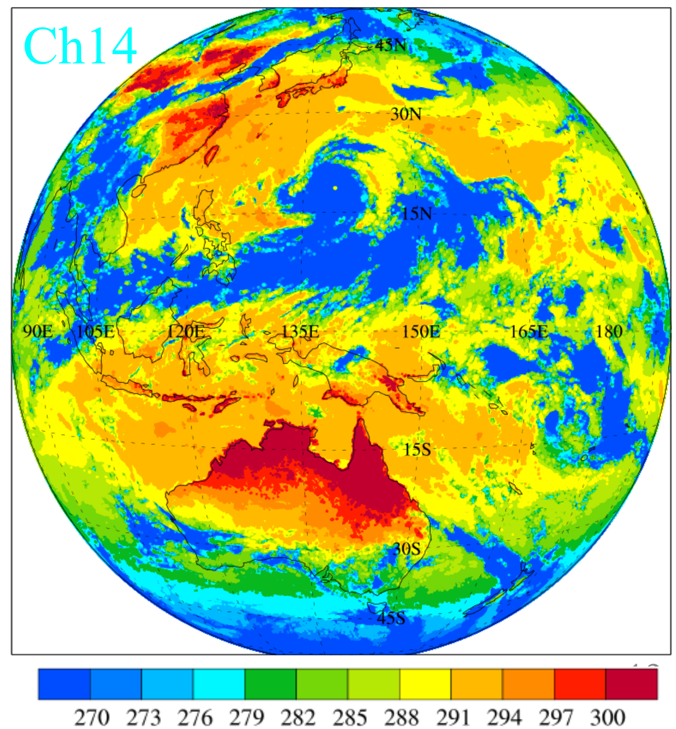

Brightness Temperatures of AHI Ch14

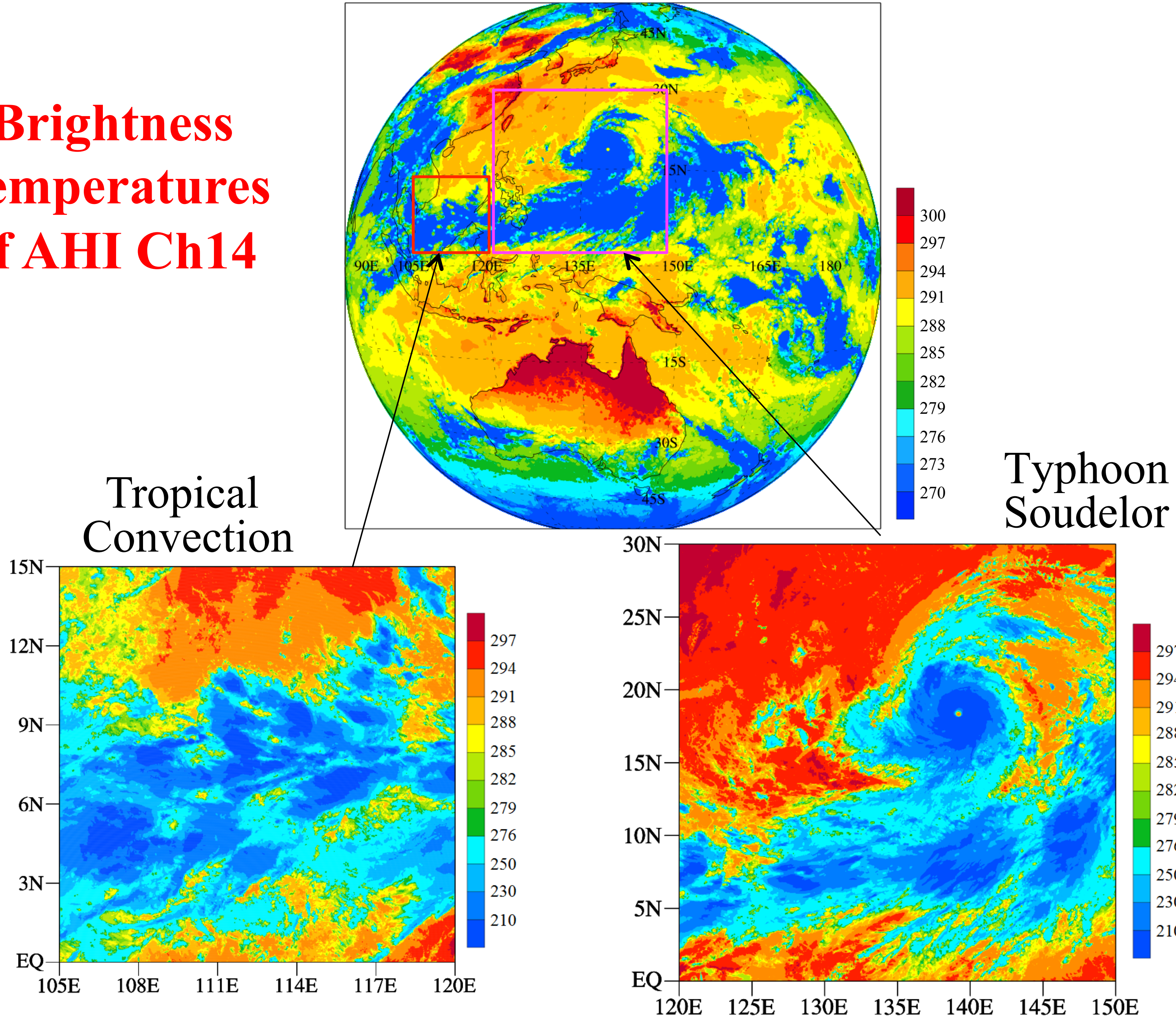

Cloud Mask within Typhoon Soudelor (1/2)

ETROP

Channel 14 Emissivity Referenced to the Tropopause

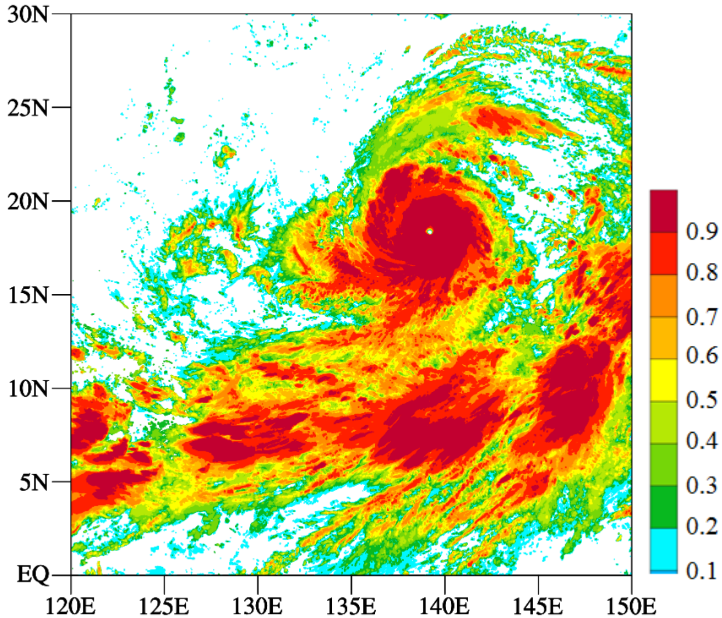

EMISS

Emissivity Test at $4\mu m$

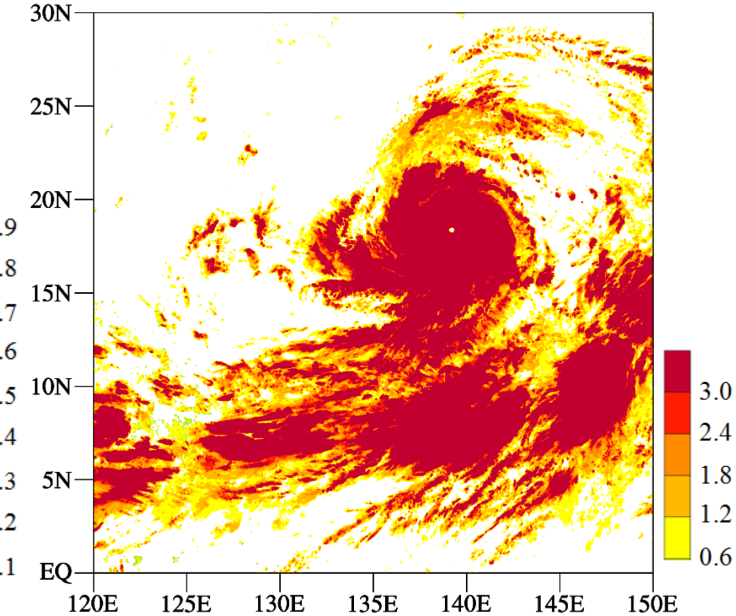

CIRH2O

Cirrus Water Vapor Test

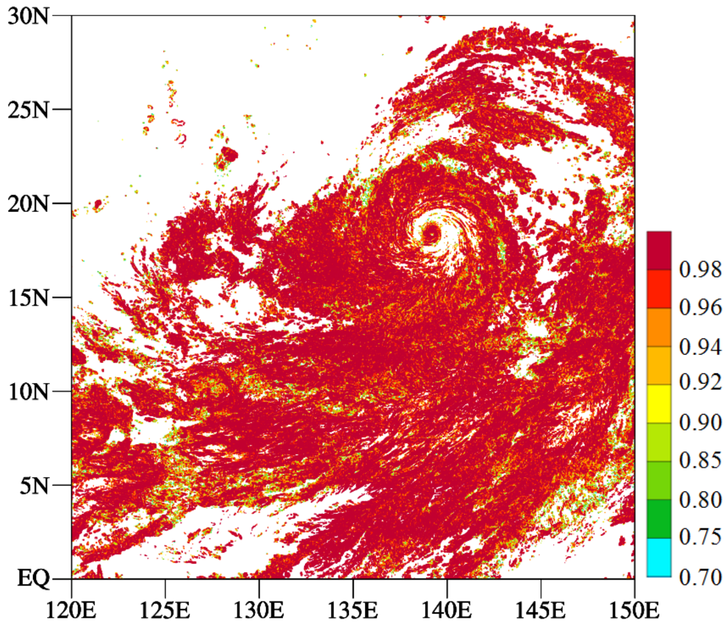

NFMFT

Negative Four Minus Five Test

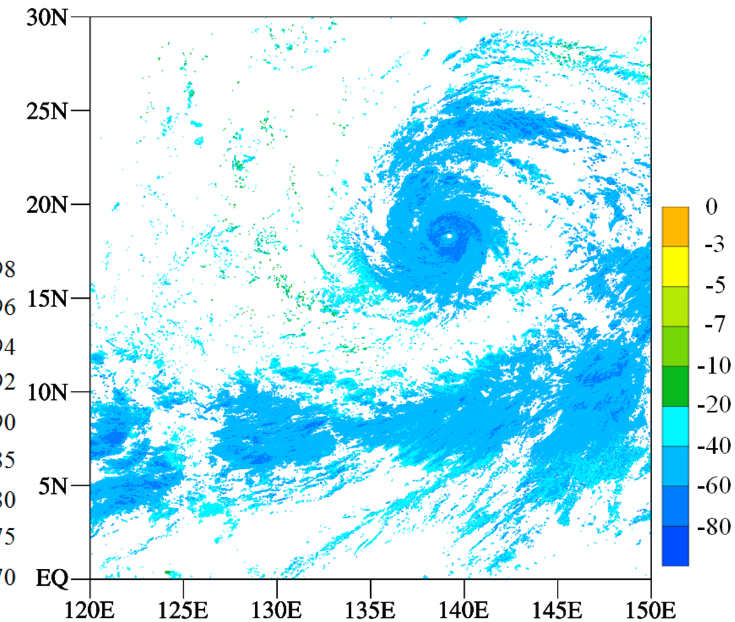

Heidinger A. (2012), ATBD: ABI Cloud Mask

Cloud Mask within Typhoon Soudelor (2/2)

TUT

Thermal Uniformity Test

RFMFT

Relative Four Minus Five Test

TEMPIR

Temporal Infrared Test

RTCT

Relative Thermal Contrast Test

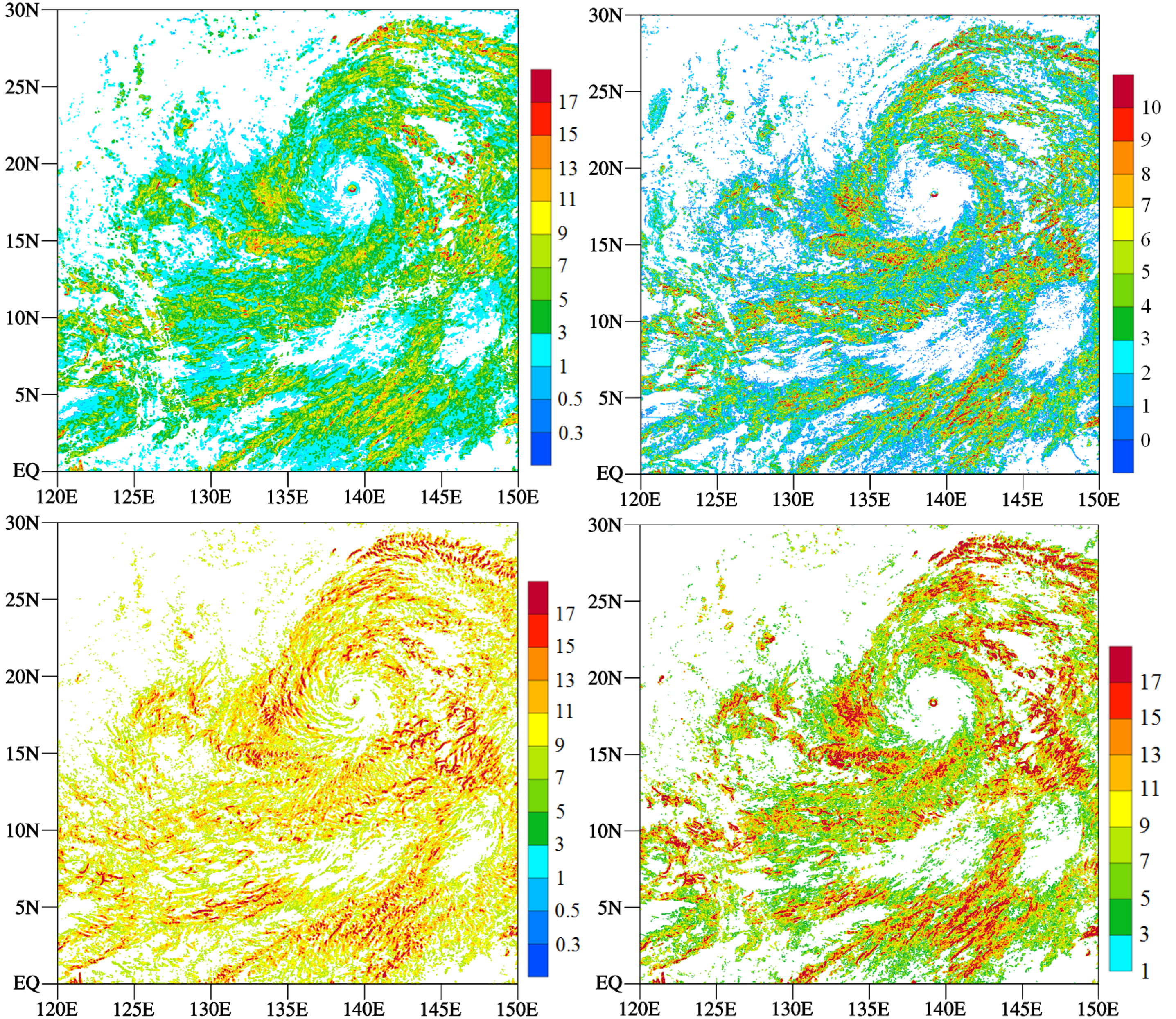

Heidinger A. (2012), ATBD: ABI Cloud Mask

Cloud Mask within Tropical Convection (1/2)

ETROP

EMISS

CIRH2O

NFMFT

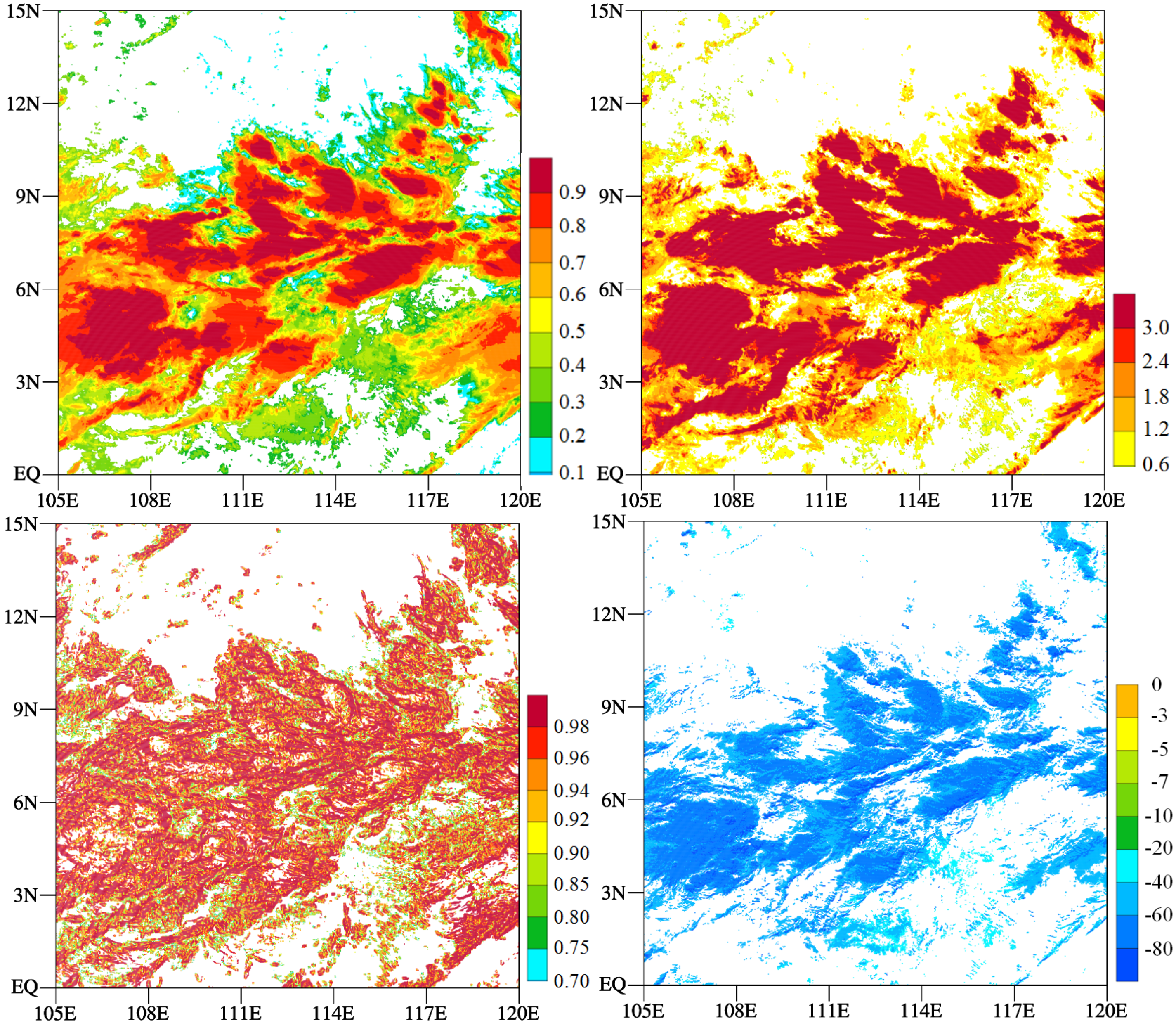

Cloud Mask within Tropical Convection (2/2)

TUT

RFMFT

TEMPIR

RTCT

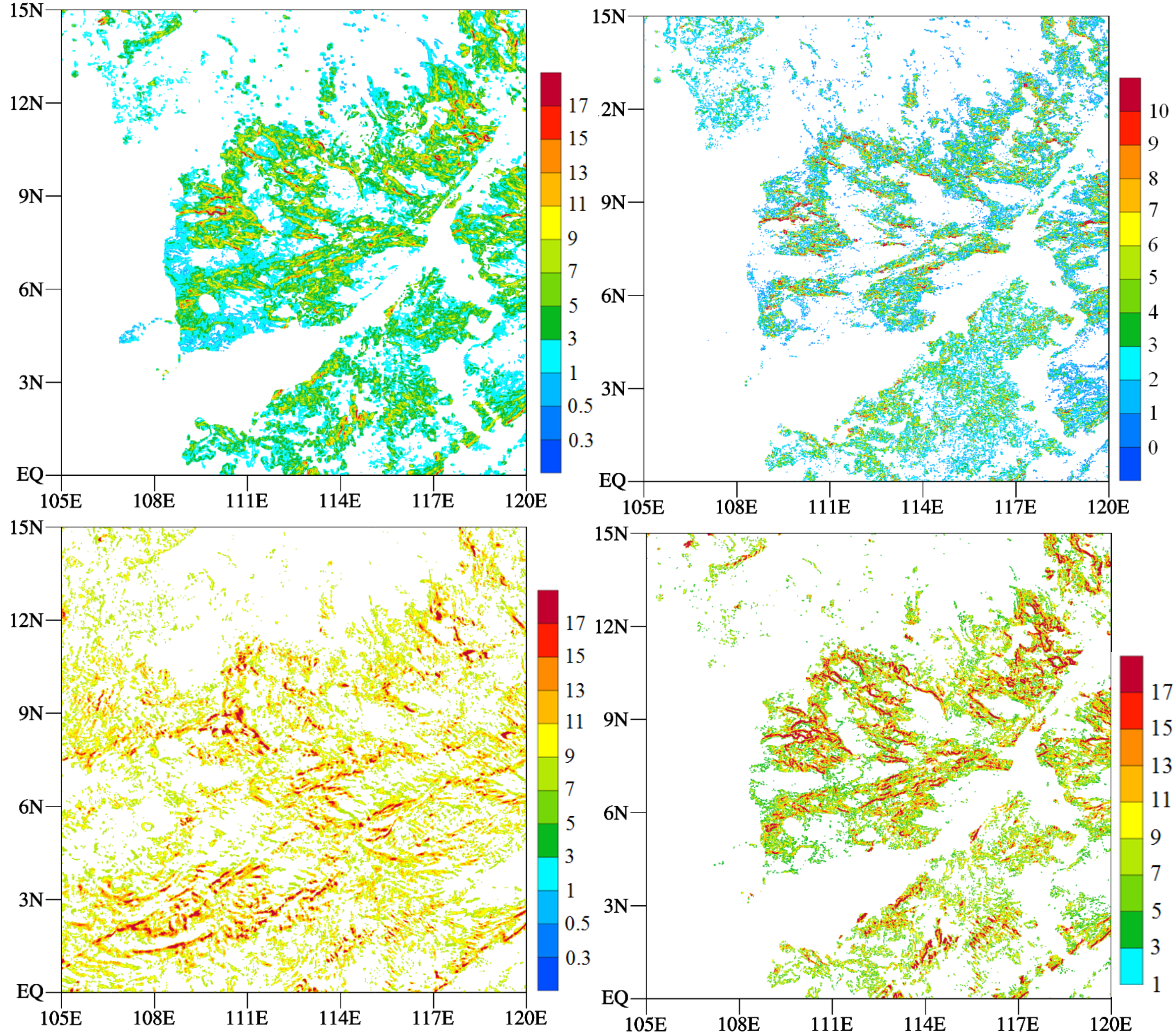

Comparison between Two Different Cloud Masks

Typhoon Soudelor | **Tropical Convection**

ETROP

Channel 14 Emissivity Referenced to the Tropopause

RFMFT

Relative Four Minus Five Test

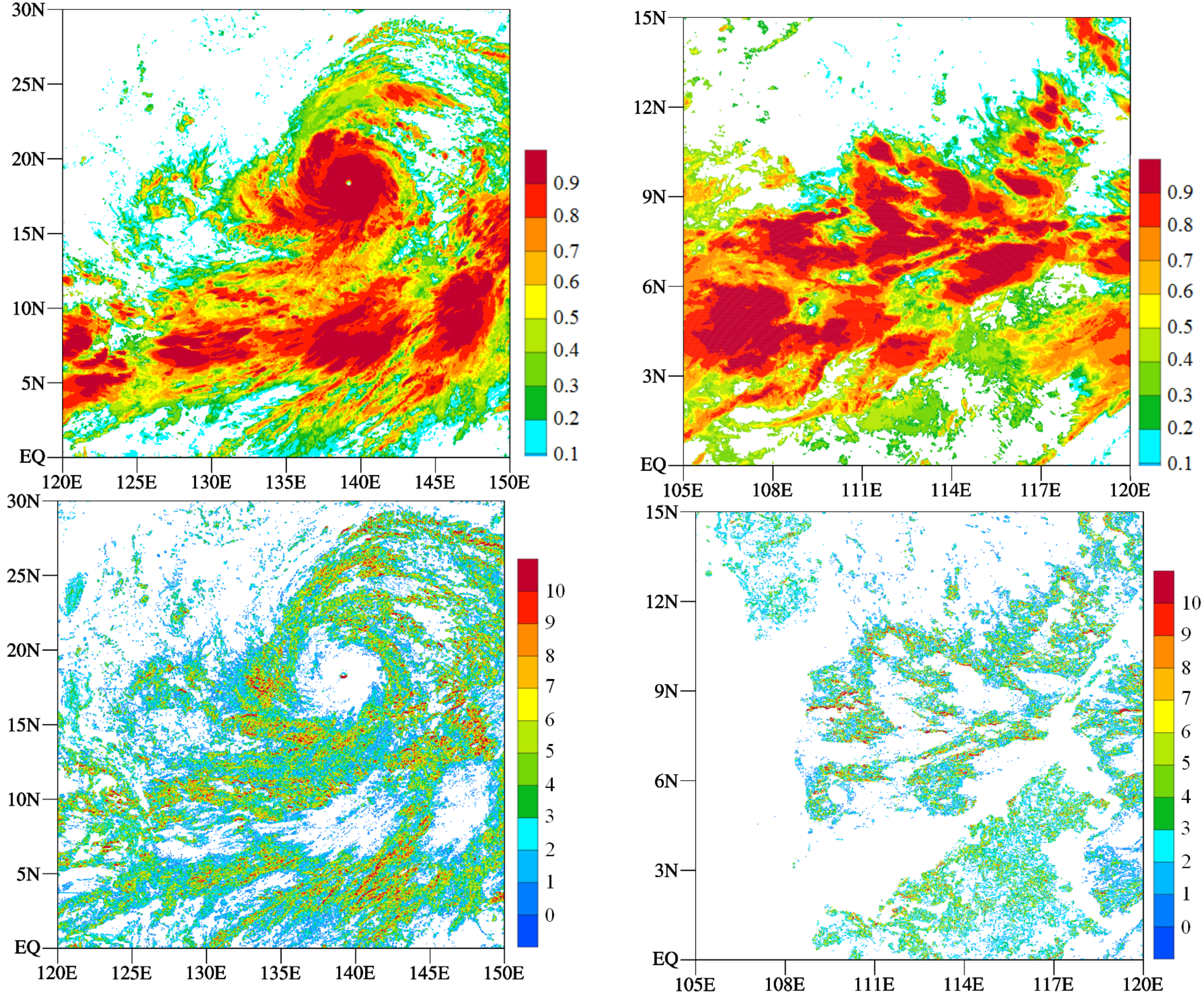

Comparison of Cloud Mask between Two Methods

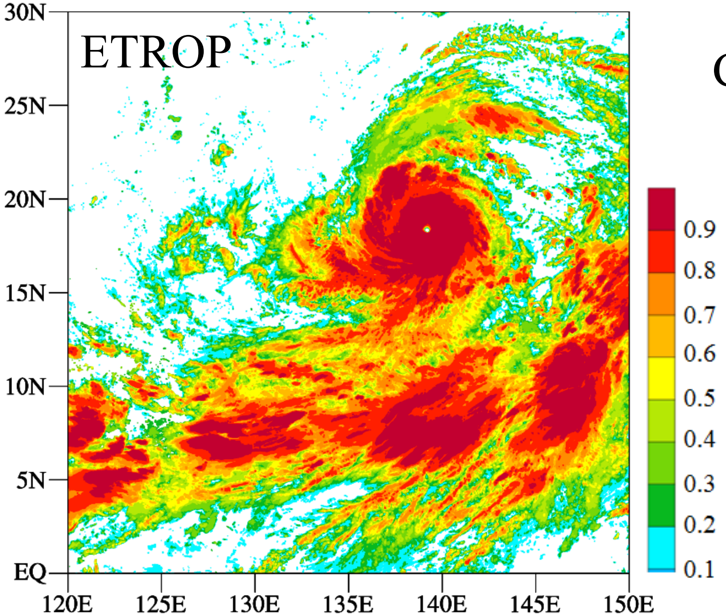

Channel 14 Emissivity Referenced to the Tropopause

$$\varepsilon_{ETROP} = \frac{I^{obs}_{11.2\mu m} - I^{CRTM}_{clear-sky}}{I_{blackbody} - I^{CRTM}_{clear-sky}}$$

The ETROP test assumes that clouds produce colder 11.2 μm brightness temperatures than what would have been observed under clear-sky conditions.

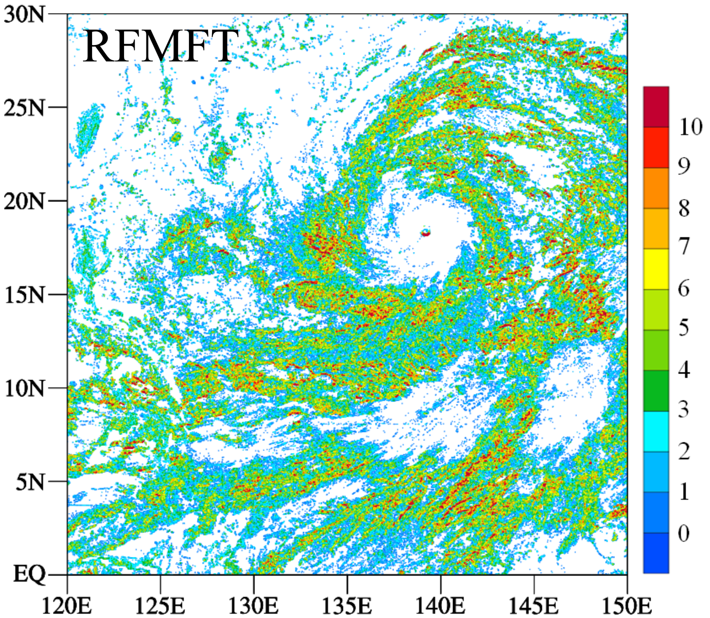

Positive Four Minus Five Test

$$\chi_{RFMFT} = \max_{5x5} \Delta I^{obs,NWC}_{11.2-12.3} - \Delta I^{CRTMclear-sky}_{11.2-12.3}$$

$$\Delta I^{obs}_{11.2-12.3} = I^{obs}_{11.2\mu m} - I^{obs}_{12.3\mu m}$$

$$\Delta I^{CRTMclear-sky}_{11.2-12.3} = I^{CRTMclear-sky}_{11.2\mu m} - I^{CRTMclear-sky}_{12.3\mu m}$$

The basis for the RFMFT test is the variation in $\Delta I^{obs}_{11.2-12.3}$ for cloudy conditions.

Overlap of Cloudy Pixels Found by Nine Cloud Masks

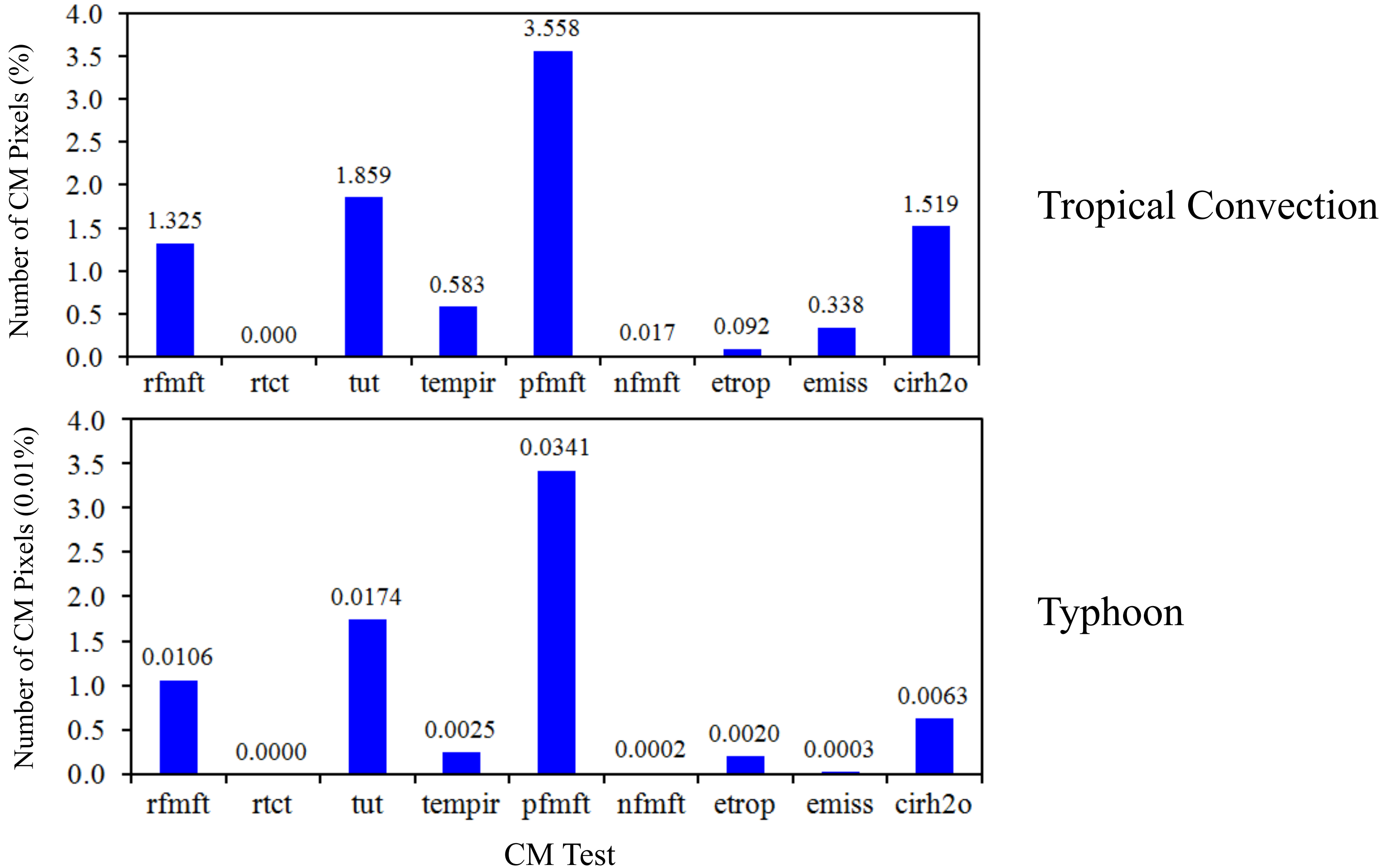

Percentage of cloudy pixels detected by one CM but not by any other CMs for AHI data within two selected regions (105E-120E, 0-15N; 120E-150E, 0-30N) at 0130 UTC August 4, 2015. The total number of cloudy pixels within the two regions detected by nine CMs are 551,384 and 2,382,845.

AHI Observed and CRTM/ ECMWF Simulated Brightness Temperatures of Channel 16 in Clear-Sky Conditions

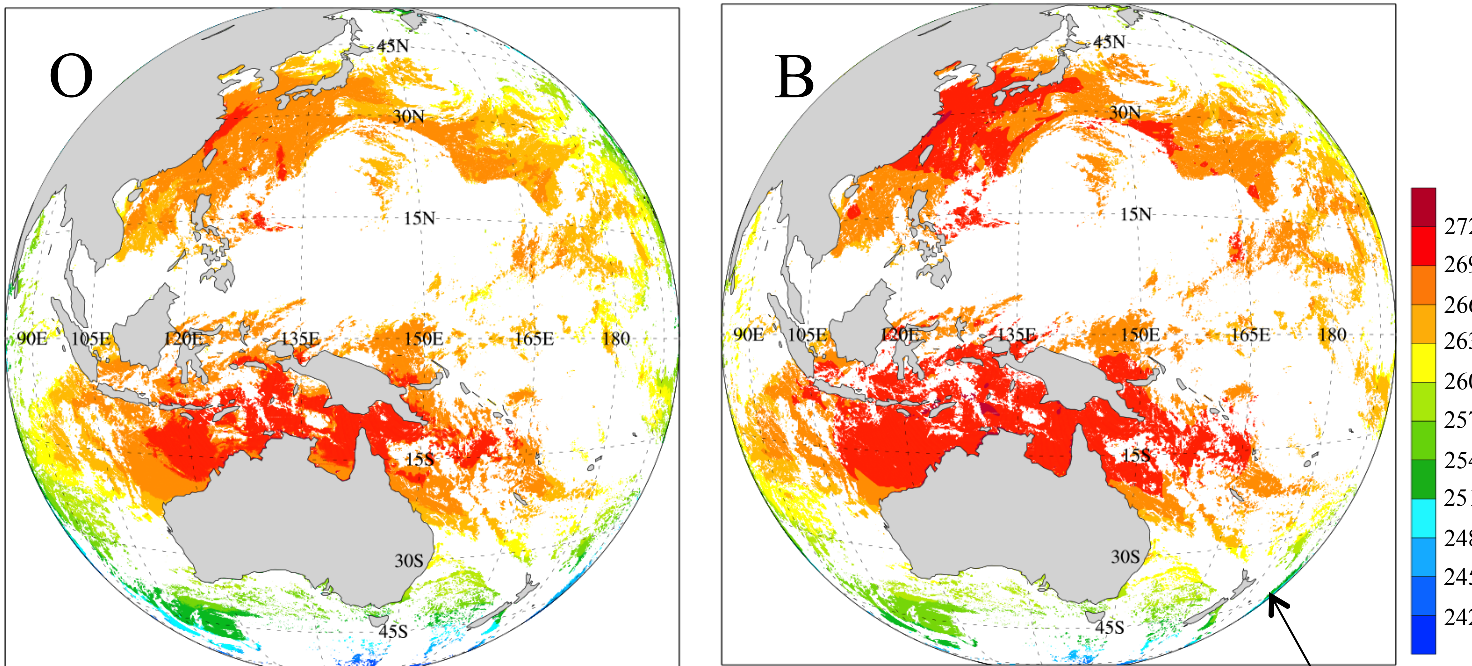

CRTM/ECMWF

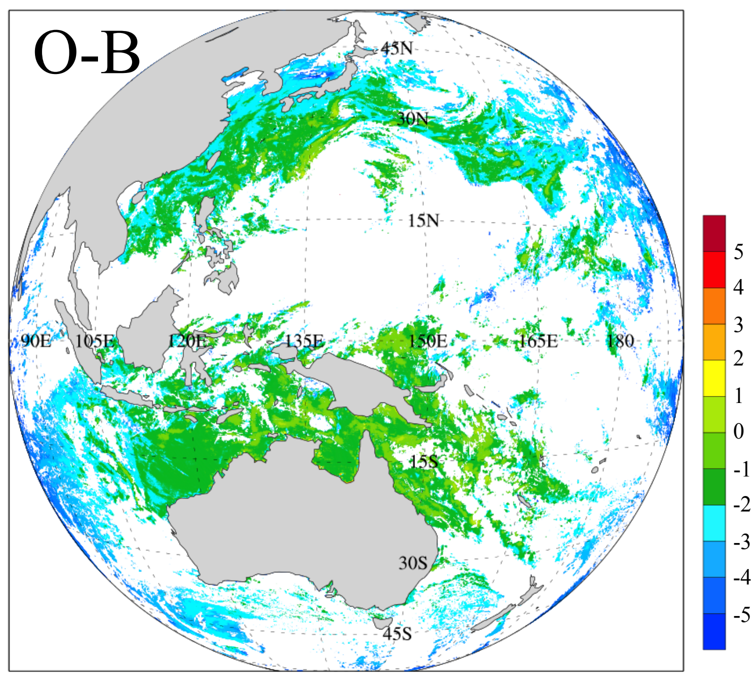

0130 UTC
August 4, 2015

Bias and Standard Deviation between AHI Observations and CRTM/ECMWF Simulations

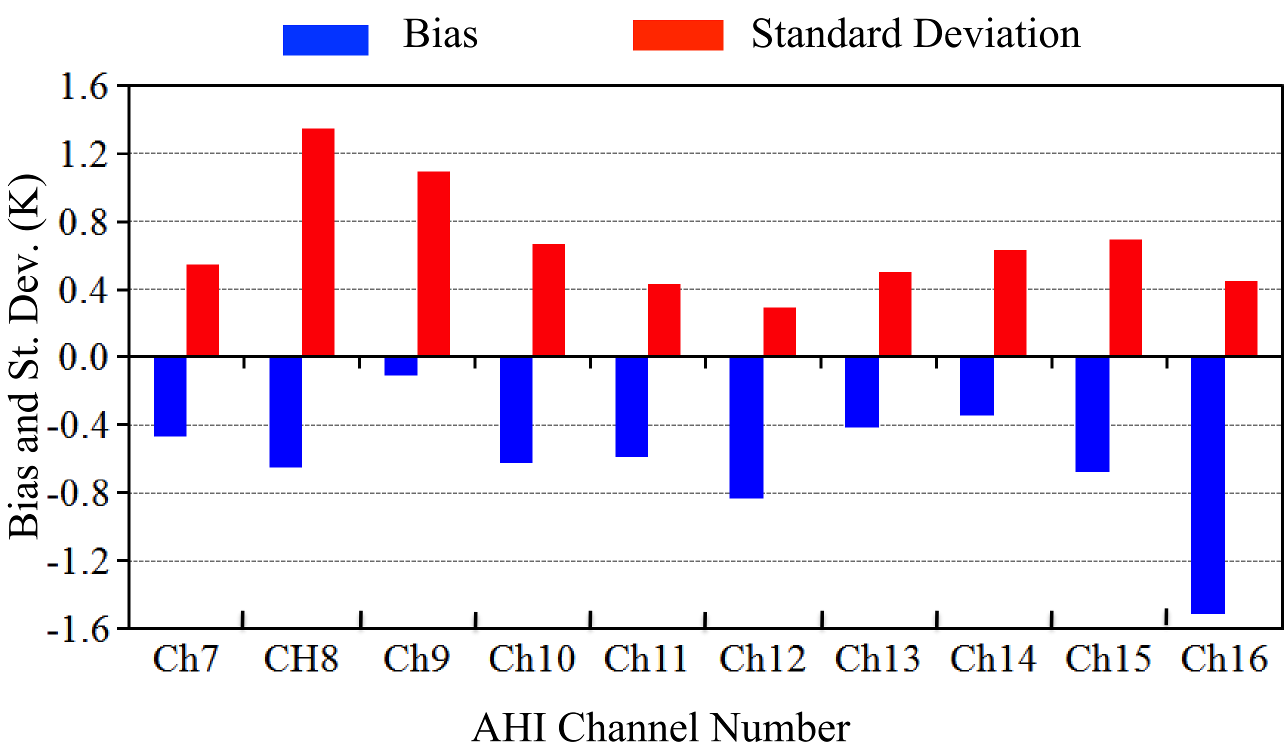

Channel	Bias (K)	Std. (K)
7	-0.47	0.54
8	-0.65	1.34
9	-0.11	1.09
10	-0.62	0.67
11	-0.58	0.43
12	-0.83	0.29
13	-0.41	0.50
14	-0.34	0.63
15	-0.67	0.69
16	-1.51	0.44

All clear-sky data with satellite zenith angle being less than 25° over ocean in clear-sky conditions on August 4, 2015 at half-hour interval.

Estimated AHI O-B Biases and Standard Deviations

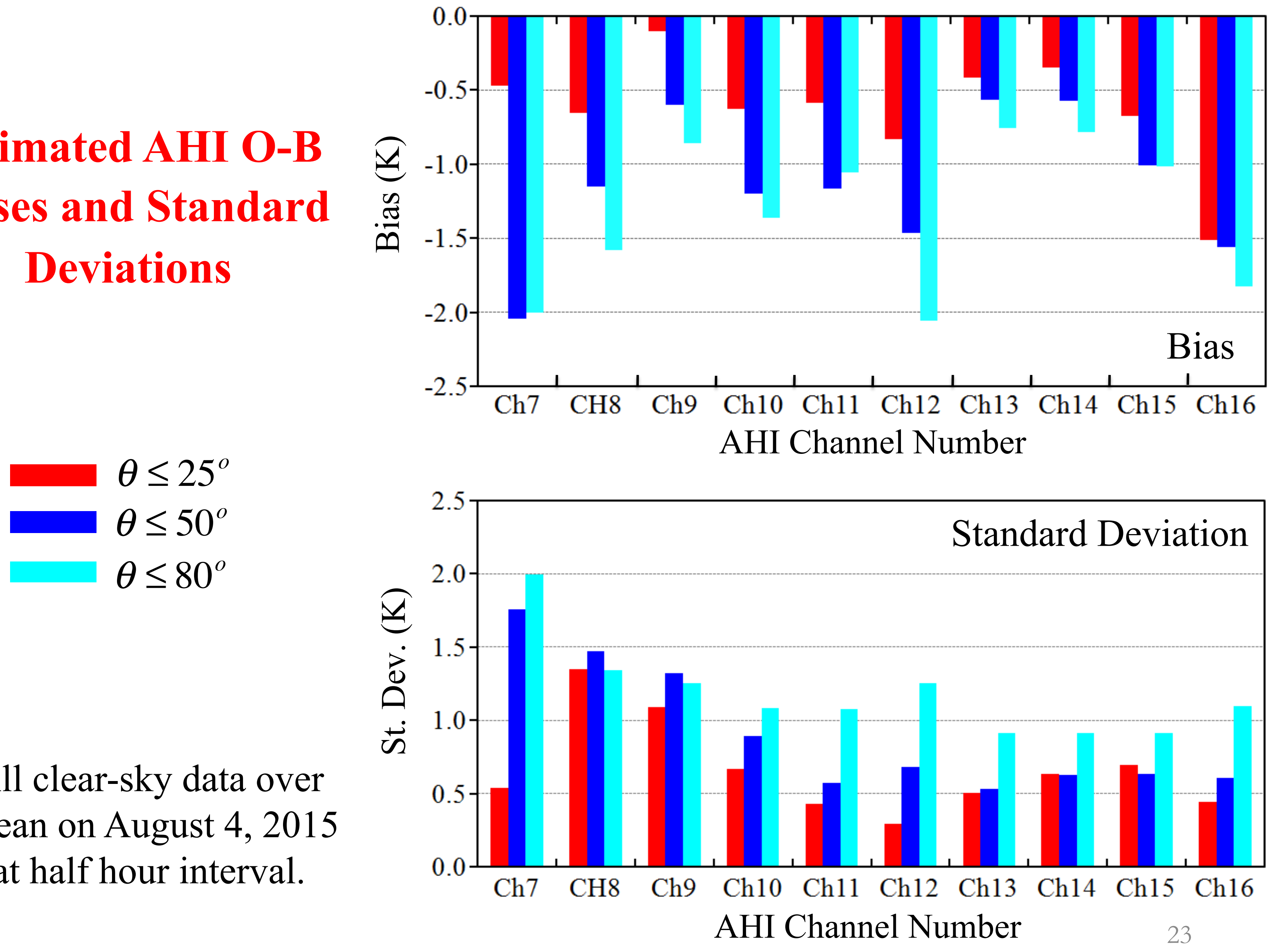

All clear-sky data over ocean on August 4, 2015 at half hour interval.

Bias and Standard Deviation between AHI Observations and CRTM/ECMWF Simulations

Channel Number	Bias (K)			Std. (K)		
	$\theta \le 25^o$	$\theta \le 50^o$	$\theta \le 80^o$	$\theta \le 25^o$	$\theta \le 50^o$	$\theta \le 80^o$
7	-0.47	-2.04	-2.00	0.54	1.75	1.99
8	-0.65	-1.15	-1.58	1.34	1.47	1.34
9	-0.11	-0.60	-0.86	1.09	1.32	1.25
10	-0.62	-1.20	-1.36	0.67	0.89	1.08
11	-0.58	-1.16	-1.06	0.43	0.57	1.07
12	-0.83	-1.46	-2.05	0.29	0.68	1.25
13	-0.41	-0.56	-0.76	0.50	0.53	0.91
14	-0.34	-0.57	-0.78	0.63	0.62	0.91
15	-0.67	-1.00	-1.01	0.69	0.63	0.91
16	-1.51	-1.55	-1.82	0.44	0.61	1.09

All data at half-hour interval over ocean in clear-sky conditions on August 4, 2015.

AHI O-B Bias Dependence on Zenith Angle

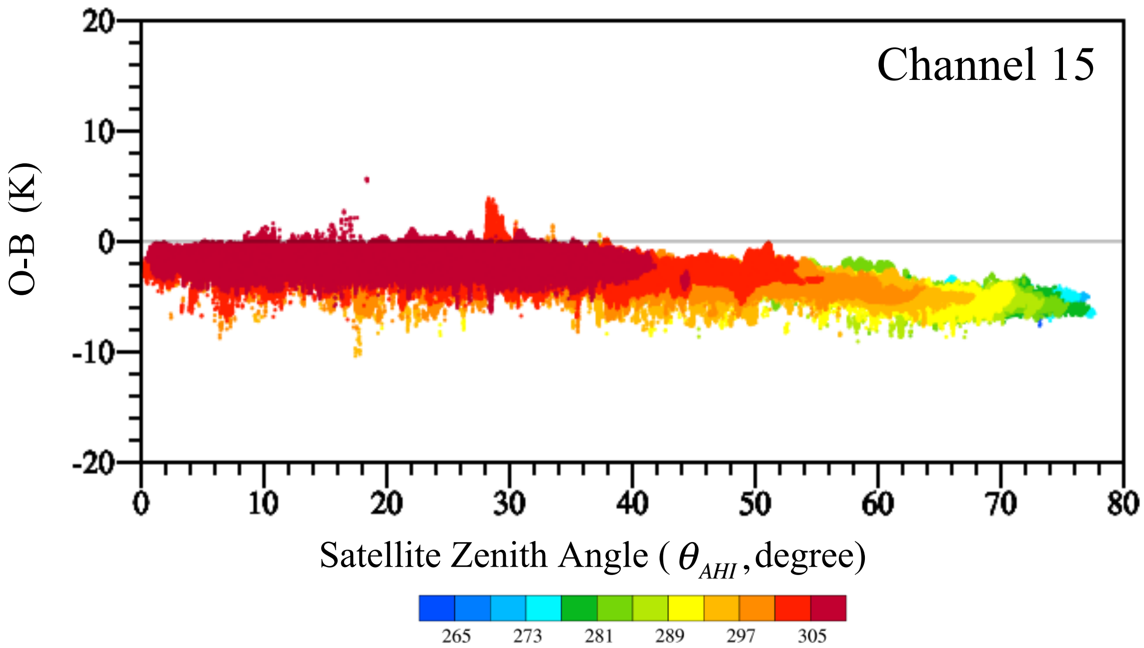

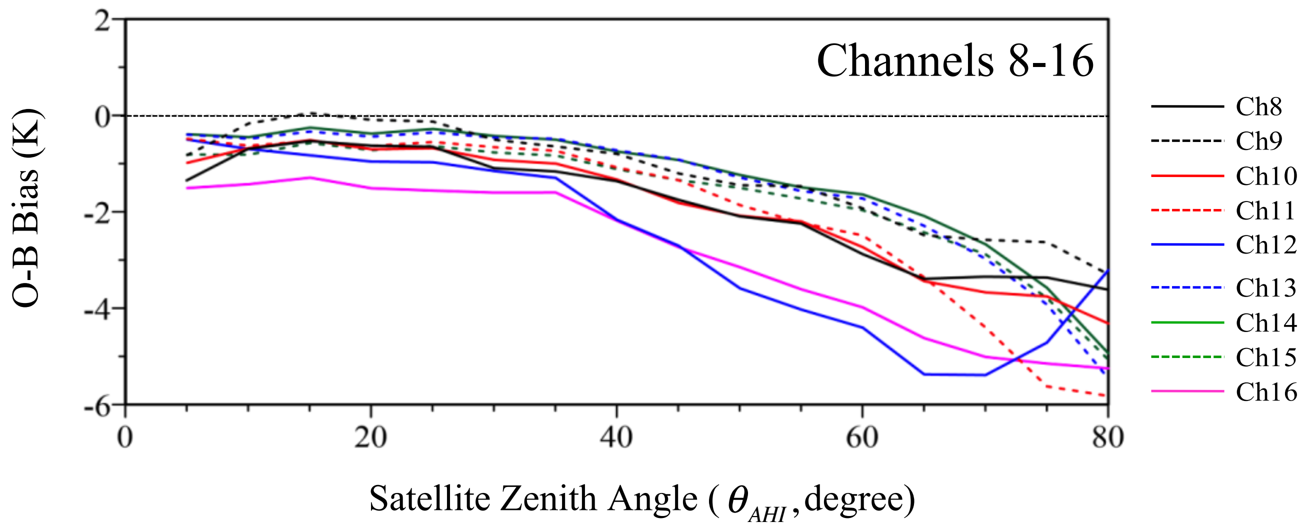

Spatial Distribution of AHI O-B Bias of Channel 16

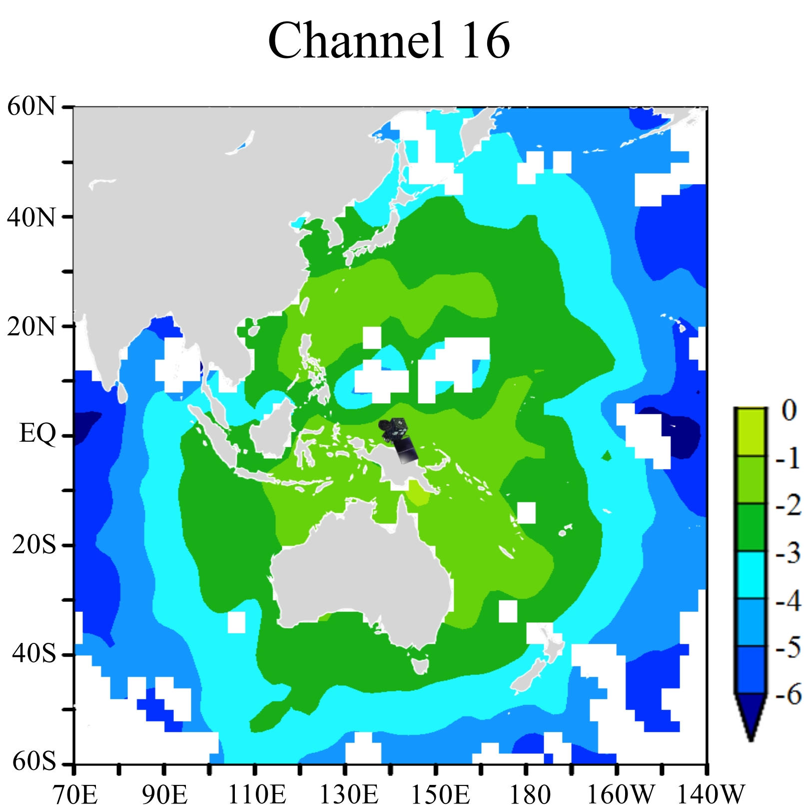

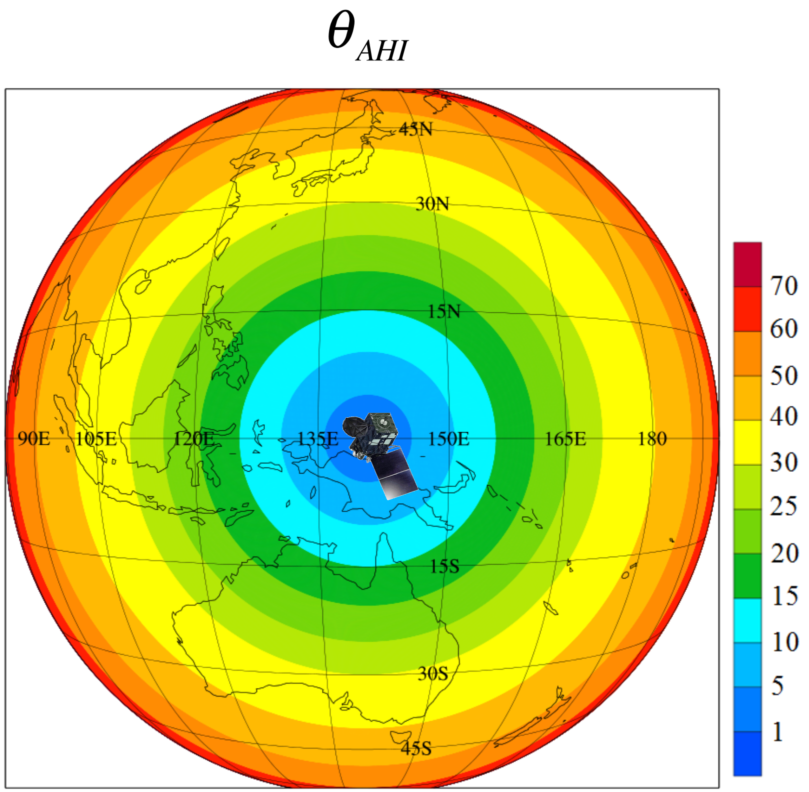

- The AHI O-B bias increases with satellite zenith angle
- The O-B bias of AHI channel 16 increases from zero to about 6 K when the satellite zenith angle changes from zero to more than 70^{o}

All clear-sky data over ocean on August 4, 2015 at half hour interval.

O-B Biases of AHI Channel 8-11

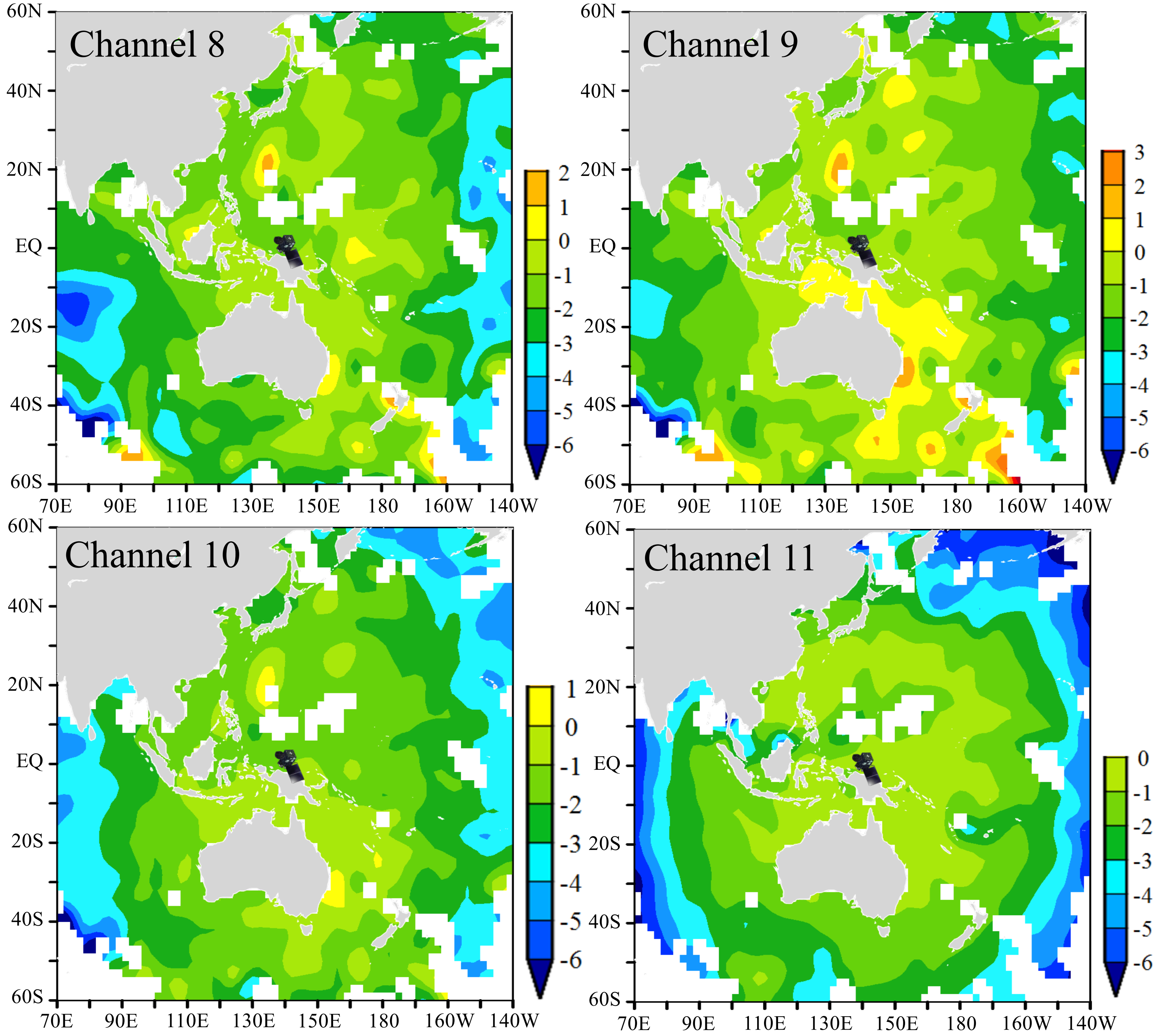

O-B Biases of AHI Channel 12-15

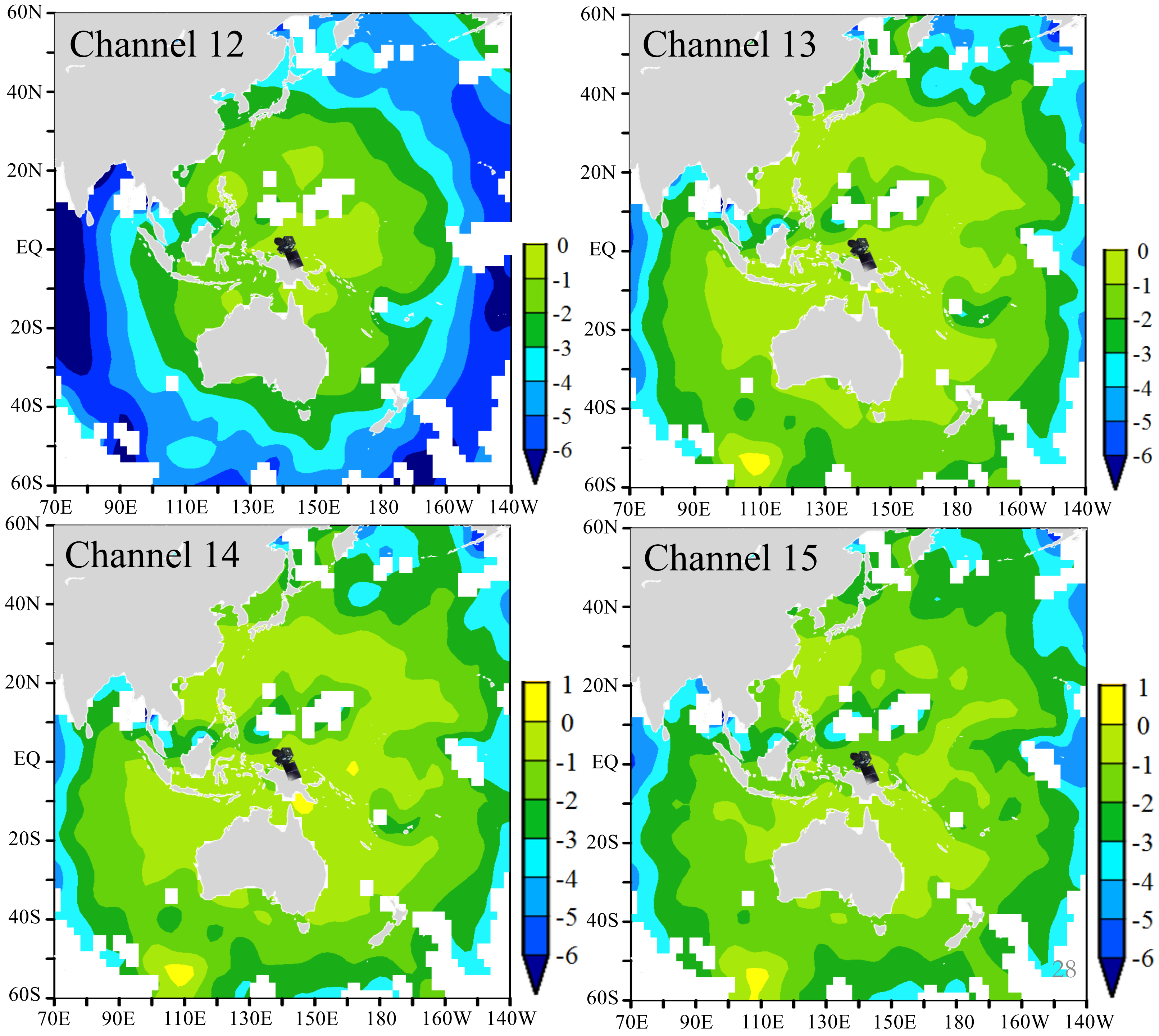

Spatial Distribution of AHI O-B Bias and Standard Deviation of Channel 16

- Zenith dependent bias is independent of data count distributions
- Standard deviation is usually larger when data counts are smaller

All clear-sky data over ocean on August 4, 2015 at half hour interval.

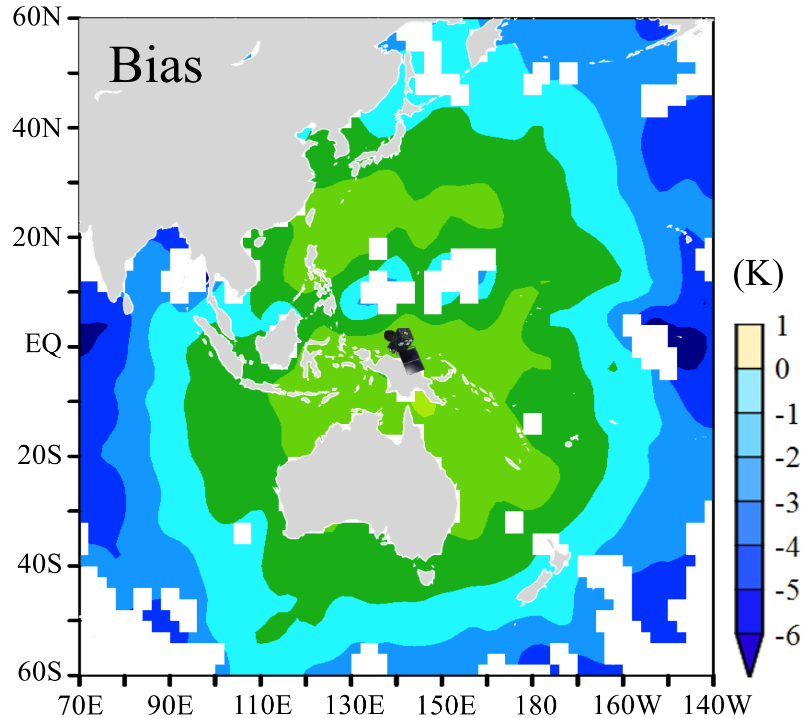

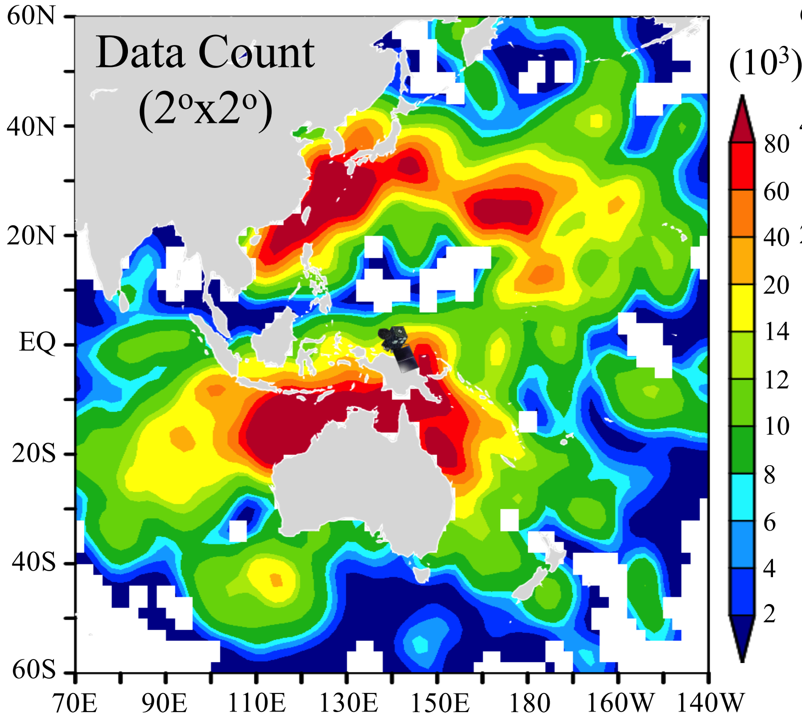

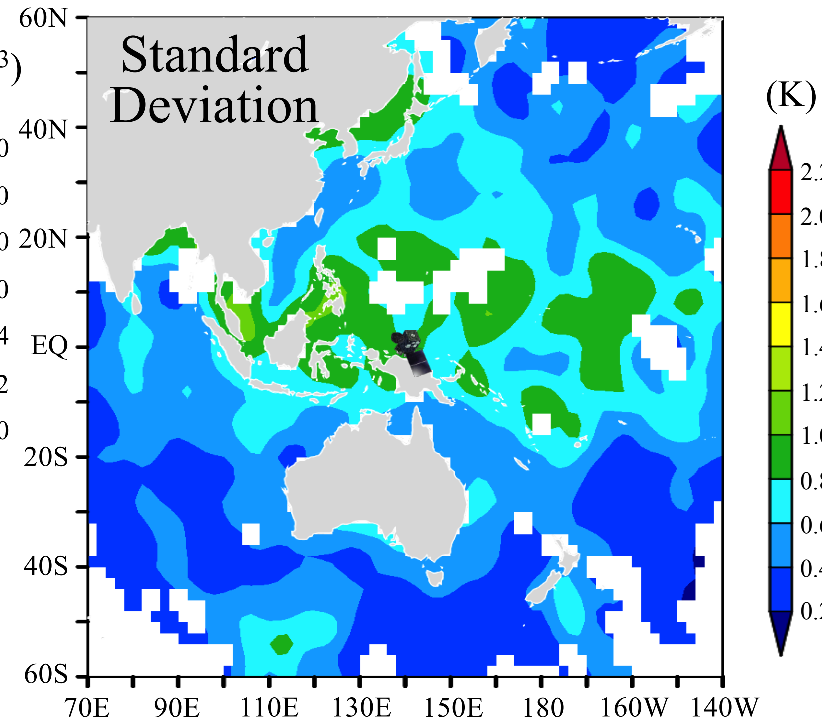

Summary and Conclusions

- Assimilation of GOES imager radiance in HWRF resulted in improvements in hurricane track and intensity forecasts and coastal QPFs
- GOES-R AWG cloud mask algorithm is fully vetted in the baseline HWRF/DA system for quality control of clear-sky radiance assimilation
- The bias of AHI radiance data is evaluated with respect to the ECMWF forecast fields. In clear-sky conditions, O-B bias is dependent on scan angle
- Future AHI data assessment will be extended to cloudy conditions and O-B bias features will be separately characterized according to different cloudy types and surface conditions.